Electronic Supplementary Material (ESI) for Chemical Communications

Electrochemical intermediate species and reaction pathway in H_2 oxidation on solid electrolytes

(Supporting Information)

Farid El Gabaly,*,† Anthony H. McDaniel,† Michael Grass,‡ William Chueh,†

Hendrik Bluhm,¶ Zhi Liu,‡ and Kevin F. McCarty†

Sandia National Laboratories, CA 94550, USA, Advanced Light Source, Lawrence Berkeley National Laboratory, CA 94720, USA, and Chemical Sciences Division, Lawrence Berkeley National Laboratory, CA 94720, USA

E-mail: felgaba@sandia.gov

Materials and Methods

The electrochemical device (Figure 1C) consisted of patterned Pt (99.995% pure) electrodes evaporated onto a (100) single-crystal YSZ ($Y_{0.16}Zr_{0.84}O_{1.92}$) wafer 0.5 inch diameter and 0.5 mm thick (MTI Corporation). The Pt film was 250 nm thick. A 5 nm Ti layer was used to improve the Pt adhesion to the YSZ. Ti reacts with the YSZ and is not observed by XPS. At measurement conditions, the Pt electrodes were fully dense. The Y doping was 8 mol %, giving high oxygen-ion conductivity at high temperature (0.1 Scm^{-1} at 1000°C[1]). XPS survey spectra did not show any impurity on the Pt. On the YSZ, only relatively small silicon and carbon contamination peaks

*To whom correspondence should be addressed
†Sandia National Laboratories, CA 94550, USA
‡Advanced Light Source, Lawrence Berkeley National Laboratory, CA 94720, USA
¶Chemical Sciences Division, Lawrence Berkeley National Laboratory, CA 94720, USA

were present. The full sample preparation details have been given elsewhere.[2] A special holder[3] heated the sample and contacted the Pt electrodes using tungsten probes coated with Au/Pd. A computer-based Gamry potentiostat (model PCI4-750) was used to bias the device and perform standard electrochemical tests. The experiments were performed at two different temperatures. At the lower temperature (550°C), the slower kinetics gave the adsorbates longer residence times, aiding spectroscopic identification. The higher cell currents at the higher temperature (750°C) gave better statistics for experiments dedicated to studying the charge-transfer reaction kinetics.

Spatially-resolved EC-XPS measurements were carried out at the Advanced Light Source synchrotron (LBNL, Berkeley) beamline 9.3.2.[4–7] Near-ambient pressure XPS[7,8] allows studying exposed interfaces in operando, i.e., at relevant temperature, pressure, and electrical bias while electrochemical reactions HOR and WER were taking place at the interfaces. The lateral spatial resolution of the XPS characterization was $\sim$20 μm. The photon energy was 490 eV. The peaks were Shirley-background corrected and fitted using standard XPS data analysis techniques to determine their kinetic energies. To quantify the hydroxyl XPS peak at different positions and conditions, normalization to the YSZ lattice oxygen, peak (c) in Figure 2A, was used to correct for variations in the detector response in the spatially resolved dimension. For display purposes, the binding energies of the O 1s spectra at different bias shown in Figure 2B-D are adjusted to keep the Zr $3d_{5/2}$ peak at 183 eV.

In principle, the concentration of polar or charged adsorbates could change if the potential at the surface changes. In our case, however, the applied bias produces an electric double layer only at the buried interface between YSZ and Pt. Although the YSZ potential changes with applied bias, the potential is almost constant between the Pt electrodes (Figure S1) and cannot explain the localized hydroxyl concentration changes near both Pt electrodes. Multiple studies[9–17] have predicted the existence of adsorbed hydroxyl under similar conditions.

Positions (10) and (1), where hydroxyl concentration changes were measured, correspond roughly to the Pt/YSZ interface. One key question is now whether the bias-sensitive OH resides on the YSZ electrolyte or the Pt electrodes. The Pt/YSZ boundary is not perfectly sharp.[3,18] To

discriminate between species on the electrode and electrolyte, we use a method that combines the chemical sensitivity of XPS and its capability to measure shifts in electric potential. When an electrical bias is applied to the cell, the potential drop across the electric double layer (at the interface between the YSZ and the Pt) shifts. Accordingly, the Pt and the adjacent YSZ will be at different potentials, with the difference being the magnitude of the electric double layer. Adsorbed species on Pt and YSZ are at the electrical potential of their respective substrates. We first measure the potential of the Pt electrode and the adjacent YSZ electrolyte from the bias-induced shifts of the Pt 4f and Zr 3d core-level photoelectron peaks, respectively. We then compare these shifts to the shifts of the peaks corresponding to surface hydroxyl, lattice oxide in YSZ, and oxygen on Pt (as seen in Figure 2A). Consistently, the O 1s peak associated with oxygen on Pt shifted rigidly with the Pt 4f. However, because the hydroxyl component (and the lattice oxide in YSZ) shifted rigidly with the Zr 3d peak, we know that the OH is on the YSZ.

To convert the total cell current, I_{cell}, to current density, i, we use 200 μm as the width of the triple-phase boundary based on scanning electron microscopy of the Pt/YSZ interface. The somewhat asymmetric hydroxyl concentration change between positions (1) and (10) is likely due to small variations in the electrode/electrolyte structure that lead to different overpotentials and local reaction rates. Another possibility is that positions (1) and (10) are sampling slightly different portions of the active reaction zones. The gas-phase water peak shown in Figure 2B, C, and D is not expected to change with spatial position. The gas-phase water peak at position (1) appears to be bigger than at position (10) because the former probes less YSZ (more Pt), so the water O 1s peak looks relatively larger.

Determination of the Reaction Kinetic Parameters from the Measured Overpotentials

The overpotentials are directly determined using the energies of the photoelectron peaks (which gives the local electric potentials of the near surface[2,3]). YSZ electrolyte and Pt electrode potentials were measured using the Zr $3d_{5/2}$ and Pt $4f_{7/2}$ XPS core levels, respectively. At each analysis

location, the kinetic energies of core-level peaks with and without applied bias ($E^{\text{bias}}_{\text{K.E.}}$ and $E^{\text{eq}}_{\text{K.E.}}$, respectively) are subtracted to obtain the change in the material's inner electric potential, $\Delta\phi$, i.e.,

$$E^{\text{bias}}_{\text{K.E.}} - E^{\text{eq}}_{\text{K.E.}} = -\Delta\phi \quad \text{(in eV)}. \tag{S1}$$

The overpotential η at an interface is then the difference between the inner potential changes of the electrode and the adjacent electrolyte:[2]

$$\eta = \Delta\phi^{\text{electrode}} - \Delta\phi^{\text{electrolyte}}. \tag{S2}$$

Figure S1 shows the potential landscape between the Pt electrodes for several applied biases.

To extract the kinetic parameters of the multistep reaction, the cell is modeled using a Butler-Volmer-type equation[19–22] that describes the current density ($i = I_{cell}/A$, where A is the reaction area) in terms of the overpotential and two transfer coefficients, α_f and α_r, that describe the forward (HOR) and the reverse reactions (WER), respectively. Then,

$$i = i_0 \left(\exp\left[\frac{\alpha_r F \eta}{RT}\right] - \exp\left[-\frac{\alpha_f F \eta}{RT}\right] \right), \tag{S3}$$

where i_0 is the exchange current density, F is the Faraday constant, R is the ideal gas constant, and T is the temperature. For relatively small overpotentials, we assume that the same mechanism applies for HOR and WER. For that purpose the overpotential analysis is restricted to $|\eta| < 200$ mV, or equivalently, $|V_{cell}| < 400$ mV. The transfer coefficients α_f and α_r are determined by the multistep reaction mechanism:[21]

$$\alpha_f = \frac{\overrightarrow{\gamma}}{\nu} + r\beta \tag{S4}$$

$$\alpha_r = \frac{n - \overrightarrow{\gamma}}{\nu} - r\beta, \tag{S5}$$

where n is the total number of electrons transferred in HOR and WER, $\overrightarrow{\gamma}$ is the sum of all electrons transferred before the rds, ν is the stoichiometric number of the rds step (number of times it occurs

in the net reaction), and r is the number of electrons transferred in the rds. (If $r = 1$ the rds is an electrochemical reaction and if $r = 0$ it is a chemical reaction.) β is the symmetry factor that describes the fraction of the overpotential that influences the activation energy of the rds. In this study we initially assume a symmetrical energy barrier ($\beta = 0.5$). All the kinetic reaction coefficients except β are natural numbers. After obtaining α_f and α_r from experimental data, we solve Eq. (S4) and Eq. (S5) to determine the kinetic parameters, which elucidate the mechanism.

To extract the exchange current density and the transfer coefficients from the experimental data, we rewrite[23] Eq. (S3) as:

$$\log_{10}\left(\frac{|i|}{e^{\left(\frac{n}{\nu}\frac{F}{RT}\eta\right)}-1}\right) = \log_{10}(i_0) - \alpha_f \frac{F}{2.303RT}\eta. \qquad \text{(S6)}$$

The left hand side plotted against the overpotential, η, should be linear. Figure S2 plots the HOR and WER data in this form. The slope of the linear fit gives α_f, a combination of kinetic parameters. Least-squares fits of the experimental data give α_f^{HOR}=1.1±0.2 and α_f^{WER}=1.2±0.1 (the errors are ±2 standard deviations). The linearity of the experimental data shows that the assumptions of Eq. (S3) are valid. To discover the unique values of the other kinetic parameters we need to explore the parameter space of their possible values. Eight parameters describe the mechanisms of reactions HOR and WER: n, ν, $\overrightarrow{\gamma}$, $\overleftarrow{\gamma}$ (the number of electrons transferred after the rds), r, α_f, α_r, and β. Further, we have 5 equations relating the parameters: $\beta = 0.5$ (by initial assumption), $n = 2$, $n = \overrightarrow{\gamma} + \overleftarrow{\gamma} + \nu r$, Eq. (S4), and Eq. (S5). This leaves 3 independent unknown parameters, which we choose to be ν, $\overrightarrow{\gamma}$, and r. Further limitations are dictated by the parameter definitions $r = 0$ or 1 and $0 \leq \overrightarrow{\gamma} \leq n$, i.e., $\overrightarrow{\gamma} = 0$, 1 or 2. We have simulated all possible combinations for these two parameters using the plausible assumption that $1 \leq \nu \leq 3$. We then calculated the other parameters using the relationships and simulated the cell current using Eq. (S6). A simple visual comparison of the simulated and experimental curves, such as in Figure S2, was enough to rule out all but one combination of parameters, whose transfer coefficients are $\alpha_f = 1.0$ and $\alpha_r = 1.0$. These values agree with the linear fits to the data (i.e., $\alpha_f^{HOR} = 1.1 \pm 0.2$ and $\alpha_f^{WER} = 1.2 \pm 0.1$). (The simulated

lines that gave the second best fit to the experimental data yielded transfer coefficients values of 1.5 or 0.5, which deviate substantially from the experimental values.)

The resulting parameter combination is: $n = 2$, $\nu = 1$, $\overrightarrow{\gamma} = 1$, $\overleftarrow{\gamma} = 1$, $r = 0$, $\alpha_f = 1.0$, $\alpha_r = 1.0$, and $\beta = 0.5$. The unique combination of kinetic parameters show that the rds is a chemical reaction without charge transfer ($r = 0$) that occurs once ($\nu = 1$). Additionally, one electron is transferred before ($\overleftarrow{\gamma} = 1$) and another after ($\overrightarrow{\gamma} = 1$) the rds.

To rule out the effect of the symmetry factor in the parameter exploration, we have additionally varied β between 0.3 and 0.7 for all parameter combinations and found that the same parameter set gave the best agreement with the experimental data.

Note that constructing the simulated lines in Figure S2 required multiple calculations of the current density i using Eq. (S3). The required value of i_0 was obtained from the experimental data, i.e., extracted using Eq. (S6), so the y-intercept of the simulated lines comes from the experimental data. The simulation of the exchange current density i_0 is beyond the scope of this work. Nevertheless, we remark that all the information about the kinetic parameters is contained solely in the slope of the lines and the y-intercept value is only needed to plot and compare the calculated and experimental data.

i_0 in Eq. (S3) is defined as:

$$i_0 = nF\left(-a_{A1}\,\overrightarrow{k}_{rds}\left[\prod_{i=1}^{rds-1}\frac{\overrightarrow{k}_i}{\overleftarrow{k}_i}\right]\right), \tag{S7}$$

where a_{A1} is the surface activity of the overall reaction reactant, $\overrightarrow{k}_{rds}$ is the heterogeneous rate constant of the rate determining step reaction in the forward direction at equilibrium ($\eta = 0$), and $\overrightarrow{k}_i$ and $\overleftarrow{k}_i$ are the rate constants for reaction step i in the forward and reverse directions, respectively.

The assumptions[24] made in deriving Eq. (S3) are: (i) only the rds limits the rate of the overall reaction; (ii) the rds is at least 100 times slower than all other reaction steps; (iii) the same rds applies to the forward and reverse reaction, and over the whole potential range under consideration;

(iv) all steps besides the rds are assumed to be at quasi-equilibrium; (v) no mass transfer limitations exist in the system. All of these assumptions apply at low overpotential, as analyzed here.

References

(1) Maier, J. *Physical chemistry of ionic materials : ions and electrons in solids*; John Wiley: Chichester England Hoboken NJ, 2004.

(2) El Gabaly, F.; Grass, M.; McDaniel, A. H.; Farrow, R. L.; Linne, M. A.; Hussain, Z.; Bluhm, H.; Liu, Z.; McCarty, K. F. *Physical Chemistry Chemical Physics* **2010**, *12*, 12138, 38.

(3) Whaley, J. A.; McDaniel, A. H.; El Gabaly, F.; Farrow, R. L.; Grass, M. E.; Hussain, Z.; Liu, Z.; Linne, M. A.; Bluhm, H.; McCarty, K. F. *Review of Scientific Instruments* **2010**, *81*, 086104, 8.

(4) Ogletree, D. F.; Bluhm, H.; Lebedev, G.; Fadley, C. S.; Hussain, Z.; Salmeron, M. *Review of Scientific Instruments* **2002**, *73*, 3872–3877.

(5) Salmeron, M.; Schlögl, R. *Surface Science Reports* **2008**, *63*, 169–199.

(6) Ogletree, D. F.; Bluhm, H.; Hebenstreit, E. D.; Salmeron, M. *Nucl. Instrum. Methods A* **2009**, *601*, 151–160, 1-2.

(7) Grass, M. E.; Karlsson, P. G.; Aksoy, F.; Lundqvist, M.; Wannberg, B.; Mun, B. S.; Hussain, Z.; Liu, Z. *Review of Scientific Instruments* **2010**, *81*, 053106.

(8) Bluhm, H.; Havecker, M.; Knop-Gericke, A.; Kiskinova, M.; Schlogl, R.; Salmeron, M. *Mrs Bulletin* **2007**, *32*, 1022, 12.

(9) Mizusaki, J.; Amano, K.; Yamauchi, S.; Fueki, K. *Solid State Ionics* **1987**, *22*, 323–330.

(10) Mizusaki, J.; Tagawa, H.; Isobe, K.; Tajika, M.; Koshiro, I.; Maruyama, H.; Hirano, K. *Journal of the Electrochemical Society* **1994**, *141*, 1674–1683, 6.

(11) Mizusaki, J.; Tagawa, H.; Saito, T.; Yamamura, T.; Kamitani, K.; Hirano, K.; Ehara, S.; Takagi, T.; Hikita, T.; Ippommatsu, M.; Nakagawa, S.; Hashimoto, K. *Solid State Ionics* **1994**, *70*, 52–58.

(12) Sukeshini, A. M.; Habibzadeh, B.; Becker, B. P.; Stoltz, C. A.; Eichhorn, B. W.; Jackson, G. S. *Journal of the Electrochemical Society* **2006**, *153*, A705–A715, 4.

(13) Mizusaki, J.; Amano, K.; Yamauchi, S.; Fueki, K. *Solid State Ionics* **1987**, *22*, 313–322.

(14) Bessler, W. G. *Solid State Ionics* **2005**, *176*, 997–1011.

(15) Zhu, H. Y.; Kee, R. J.; Janardhanan, V. M.; Deutschmann, O.; Goodwin, D. G. *Journal of the Electrochemical Society* **2005**, *152*, A2427–A2440, 12.

(16) Bessler, W. G.; Warnatz, J.; Goodwin, D. G. *Solid State Ionics* **2007**, *177*, 3371–3383.

(17) Goodwin, D. G.; Zhu, H.; Colclasure, A. M.; Kee, R. J. *Journal of The Electrochemical Society* **2009**, *156*, B1004–B1021.

(18) Pöpke, H.; Mutoro, E.; Luerßen, B.; Janek, J. *Solid State Ionics* **2011**, *189*, 56–62.

(19) Eyring, H. *Physical Chemistry. An Advanced Treatise. Volume IXA: Electrochemistry*; Academic Press Inc, 1970.

(20) Gileadi, E. *Electrode Kinetics for Chemists, Chemical Engineers, and Materials Scientists*; Wiley-VCH: New York, 1993.

(21) Bockris, J. O.; Reddy, A. K. N.; Gamboa-Aldeco, M. *Modern Electrochemistry 2A*; Springer: Berlin, 2000.

(22) Bard, A. *Electrochemical methods : fundamentals and applications*, 2nd ed.; Wiley: New York, 2001.

(23) Allen, P. L.; Hickling, A. *Transactions of the Faraday Society* **1957**, *53*, 1626–1635.

(24) Lefebvre, M. C. In *Modern Aspects of Electrochemistry*; Conway, B. E., Bockris, J. O., White, R. E., Eds.; Modern Aspects of Electrochemistry; Springer US, 2002; Vol. 32; pp 249–300.

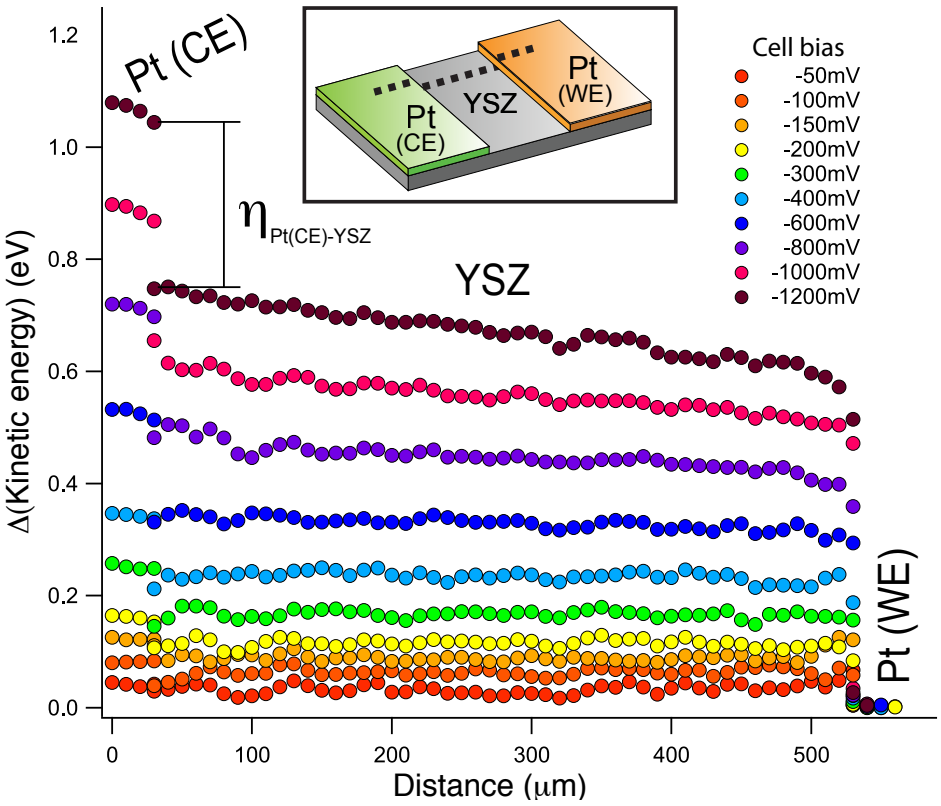

Figure S1: Overpotentials of the Pt/YSZ interfaces measured using EC-XPS. The Pt WE on the right was grounded to the XPS electron spectrometer and potentiostat. The applied potential is distributed between the drops at the two Pt/YSZ interfaces, the overpotentials, and the ohmic loss through the YSZ, which gives the sloped section. Cell at 750°C in 300 mTorr of a 1:1 mixture of H_2O and H_2. One overpotential is drawn. The inset shows the measurement path on the cell (dotted line).

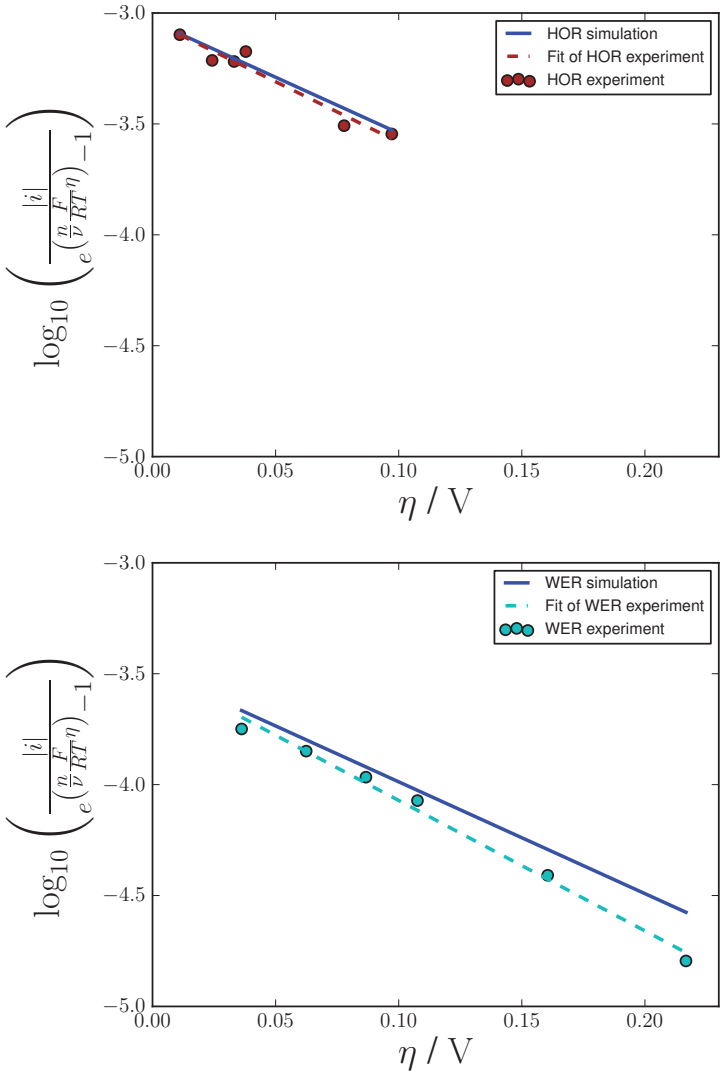

Figure S2: Normalized cell current versus overpotential for HOR (top) and WER (bottom). The experimental values are plotted as filled dots. Dashed lines represent linear fits to the experimental data, which give the forward transfer parameters: α_f^{HOR}=1.1±0.2 and α_f^{WER}=1.2±0.1. Simulated values are plotted as continuous, blue lines. The slope of the calculated lines is $\alpha_f^{HOR,sim} = 1.0$ and $\alpha_f^{WER,sim} = 1.0$. For slope comparison purposes both plots span the same ranges.